Accepted Manuscript

A chirp excitation for focussing flexural waves

Timothy P. Waters

PII: S0022-460X(18)30472-3

DOI: 10.1016/j.jsv.2018.07.028

Reference: YJSVI 14270

To appear in: *Journal of Sound and Vibration*

Received Date: 25 January 2018

Revised Date: 20 June 2018

Accepted Date: 15 July 2018

Please cite this article as: T.P. Waters, A chirp excitation for focussing flexural waves, *Journal of Sound and Vibration* (2018), doi: 10.1016/j.jsv.2018.07.028.

A chirp excitation for focussing flexural waves

Timothy P. Waters

Institute of Sound and Vibration Research

University of Southampton

Highfield

Southampton

SO17 1BJ

United Kingdom

tpw@isvr.soton.ac.uk

Declaration of Interest

The research reported in this paper forms background intellectual property to ongoing work funded by Ultra Electronics Ltd and is covered by a patent application filed jointly by University of Southampton and Ultra Electronics Ltd in 2017.

Competing interests

None

A chirp excitation for focussing flexural waves

Timothy P. Waters

Abstract

In this paper, the dispersive nature of flexural waves is exploited to generate a shock response at an arbitrary location on a waveguide. The input waveform is an up-chirp whose instantaneous frequency is chosen to ensure synchronous arrival at an arbitrary focal point. An analytical expression is derived for the required chirp waveform as a function of bandwidth and focal point location given prior knowledge of the dispersion relation.

The principle is illustrated for an analytical model of a uniform beam. Simulated results show that it is possible, in theory, to achieve peak responses that are at least an order of magnitude larger than steady state response due to harmonic excitation. Further, the peak response increases with approximately the square root of distance from the point of excitation when damping is negligible. Velocity, acceleration, normal strain and shear stress exhibit qualitatively similar results which differ quantitatively owing to their different frequency responses with respect to the input.

A single degree-of-freedom model of an electrodynamic shaker is coupled to the analytical beam model in order to predict peak mechanical responses per peak input voltage of the chirp waveform. The coupled electromechanical model is then validated experimentally through both frequency response and transient measurements. The technique is potentially applicable to situations where a large and reasonably localised transient response is required on a beam or plate-like structure using minimal instrumentation.

Keywords: chirp, flexural wave, dispersion, shock, accretion removal, ice

1. Introduction

Dispersive waves are so-called because their group velocity is frequency dependent, causing the waveform of a broadband disturbance such as a pulse to spread out as it propagates along a waveguide. This phenomenon is often undesirable, for example in ultrasonic non-destructive evaluation where overlapping wave packets scattered from different features hinder localisation of abnormalities [1]. This paper is motivated by a different intent, namely the generation of large shock responses in structures for accretion removal. Potential applications include windows, pipes, ship hulls and aircraft wings. Removal of ice from the latter has been successfully demonstrated previously using steady state rather than shock response, e.g. [2] but is limited by factors such as actuator authority and integrity. At first sight wave dispersion may also seem unbeneficial for shock based accretion removal since a shock input results in an increasingly distorted response far from the input location. However, it is shown here that by careful choice of input waveform it is possible to compensate for and even exploit dispersion to good effect. The input waveform can be arranged to launch frequency components with the correct delays for them to arrive at a target position simultaneously culminating in a large localised shock. The extended duration of the input waveform also allows far more energy to be input to the system than by an impulse.

Derivation of the necessary input waveform can be accomplished using time reversal acoustics which is an established technique for compensating for the effects of forward wave propagation [3],[4]. In time reversal acoustics, a desired response waveform at a specified point of interest is constructed in a two-step process. In the forward propagation step, a source at the point of interest excites the system using the desired response waveform, and an array of sensors is deployed to acquire a set of resulting responses due to the propagating wave field. In the backward propagation step, the measured responses are re-emitted in reverse through an array of collocated actuators in an attempt to recreate the wave field propagating in reverse time. Assuming invariance of the wave equation to time reversal, which is satisfied only for conservative systems, the response at the original source position can resemble the initial excitation waveform.

Time reversal has been applied to dispersive waves in structures at ultrasonic frequencies by Montaldo et al [5]. Longitudinal waves were excited at one end of a solid circular waveguide with a time-reversed signal so as to concentrate energy at the other end which is submersed in a fluid. A similar problem was studied by Dion et al. [6] who extracted the required input waveform from measured FRFs instead of time-reversal.

Francoeur and Berry [7] implemented time reversal on an anechoic beam at audible frequencies, principally to identify and locate wave scatterers. They used an array of PVDF sensors and piezoelectric actuators to generate an impulsive acceleration at a remote position that was larger than at the source locations.

The purpose of this paper is to quantify the potential amplification in shock response obtainable by compensating for wave dispersion, by means of a simpler approach to time reversal. A chirp (or rapid swept sine) excitation waveform is formulated given prior knowledge of the dispersion relation of a single wave type. The technique has just a forward propagation step which offers significant benefits when compared to time reversal, particularly for practical implementation:

(i) no sensor array is required (once the dispersion relation is known).
(ii) actuators are not required at the target locations.
(iii) the excitation waveform is determined analytically and is not therefore contaminated by measurement noise.
(iv) the response at the target location is filtered by the system's frequency response only once (but twice with time reversal).

However, the chirp technique accounts for neither wave reflections from boundaries, thereby focussing only incident waves, nor phase delays in the actuation system.

Section 2 of this paper presents the derivation of the chirp waveform for beams and plates in a similar form to that reported in a master's dissertation [8] from which this work originates. In section 3, a standard frequency domain analytical model of a beam is adopted from which the time response to arbitrary transient inputs can be computed via the inverse Fourier transform. The model is extended to include a coupled electrodynamic shaker for subsequent experimental validation purposes. In section 4, simulations are presented to quantify the effects of bandwidth, propagation distance and attenuation on achievable peak

responses. Section 5 concerns experimental implementation using an electrodynamic shaker, and validation of the coupled beam/shaker model developed in section 3.

2. The chirp waveform

Rapid sine sweep, or 'chirp' excitation waveforms are used in fields such as modal testing for high fidelity transfer function estimation [9] and in ultrasonic inspection to infer tone burst responses [10]. Often, a linear sweep rate is adopted on account of its flat frequency spectrum. In this paper, the sweep rate is chosen specifically to arrange for synchronous arrival of all frequency components at an arbitrary position which is remote from the input. An analytical expression is derived, based on the analysis of [8], for the case of an infinite uniform beam or plate.

A chirp signal $f(t)$ of duration T has the general form

$$f(t) = \begin{cases} F \sin \phi(t) & 0 \le t \le T \\ 0 & t > T \end{cases} \tag{1}$$

where F is a constant, φ is the instantaneous phase, and the instantaneous circular frequency ω is given by

$$\omega(t) = \frac{\mathrm{d}\phi(t)}{\mathrm{d}t} \tag{2}$$

An expression is sought for $\omega(t)$ given prior knowledge of the wave dispersion relation such that all frequency components arrive synchronously at some focal point a distance x_f from the force (or moment) at x=0. The velocity of a wave packet centred at frequency ω, is given by its group velocity,

$$c_g = \left(\frac{\mathrm{d}\left(\mathrm{Re}\{k\}\right)}{\mathrm{d}\omega} \right)^{-1} \tag{3}$$

where k is the wavenumber. At low frequencies, where the wavelength is much larger than the thickness, flexural waves are adequately described by Euler-Bernoulli theory for beams and Kirchoff-Love theory for plates. The wavenumber for propagating waves is real, if damping is neglected, and given by [11]

$$k = a\omega^{\frac{1}{2}} \tag{4}$$

where for a beam,

$$a = \left(\frac{\rho A}{EI} \right)^{\frac{1}{4}} \tag{5}$$

and for a plate,

$$a = \left(\frac{12\rho\left(1-\nu^2\right)}{Eh^2} \right)^{\frac{1}{4}} \tag{6}$$

In Eq. (5) and (6), E, ρ and ν are the Young's modulus, density and Poisson ratio, and A, I and h are the cross section area, second moment of area and thickness respectively. Substituting for k from Eq. (4) into Eq. (3) gives the group velocity for flexural waves as

$$c_g = \frac{2}{a}\omega^{\frac{1}{2}} \tag{7}$$

The time of flight (TOF) to the focal point,

$$TOF\left(\omega\right) = \frac{x_f}{c_g\left(\omega\right)} \tag{8}$$

decreases with frequency and so the instantaneous frequency of the chirp excitation must increase monotonically with time in order that lower frequencies are given a 'head start'. Denote the start and end frequencies of the chirp by $\omega_0 = \omega(0)$ and $\omega_T = \omega(T)$. Then, in order for any frequency ω to arrive at $x = x_f$ at the same instant as frequency ω_0, its launch must be delayed until time

$$t = TOF\left(\omega_0\right) - TOF\left(\omega\right) = x_f\left(\frac{1}{c_g\left(\omega_0\right)} - \frac{1}{c_g\left(\omega\right)} \right) \tag{9}$$

Substituting for the group velocity from Eq. (7),

$$t = \frac{a}{2x_f}\left(\omega_o^{-\frac{1}{2}} - \omega^{-\frac{1}{2}} \right) \tag{10}$$

Rearranging for ω gives

$$\omega(t) = \frac{1}{b_2 t^2 + b_1 t + b_0} \tag{11}$$

where

$$b_2 = \frac{4}{a^2 x_f^2} \qquad b_1 = -\frac{4}{a x_f}\omega_0^{-\frac{1}{2}} \qquad b_0 = \omega_0^{-1} \tag{12}$$

The instantaneous phase is obtained by integrating the instantaneous frequency,

$$\phi(t) = \int_0^t \frac{1}{b_2 t^2 + b_1 t + b_0} dt = 2\left(\frac{1}{b_1} - \frac{1}{2b_2 t + b_1}\right) \tag{13}$$

In practice, it can be beneficial to precede the chirp by a linear ramp of duration *n* cycles to reduce unwanted transients in the response, i.e.

$$f(t) = \begin{cases} \dfrac{t}{T_r} F \sin \omega_0 t & 0 \le t \le T_r \\ F \sin \phi(t) & T_r \le t \le T_r + T \\ 0 & t > T_r + T \end{cases} \tag{14}$$

where $T_r = \dfrac{2\pi n}{\omega_0}$ is the duration of the ramp.

Note that the premise of Eq. (9) ensures that the various frequency components arrive at the designated point simultaneously, but not that they do so at a wave crest. Consequently, the intended focal point may not coincide exactly with the point of maximum response.

3. Modelling

The preceding analysis and resulting chirp waveform are applicable to low frequency excitation of either beams or plates by adoption of the appropriate dispersion relation. Hereafter, this paper focuses on beams which differ qualitatively from plates principally in that they do not exhibit geometric wave spreading. A simple frequency domain analytical model is adopted for an infinite beam, and this is coupled to a single degree-of-freedom electromechanical model of an electrodynamic shaker for the purpose of subsequent experimental validation. The transient response of the beam (transverse acceleration, normal strain and shear stress) is obtainable due to either a mechanical or electrical chirp input.

3.1 Analytical beam model

The transient response of a beam at any point along its length can be straightforwardly computed in the frequency domain given expressions for transfer Frequency Response Functions (FRFs) reported in many seminal texts such as [11] or [12]. In the analysis it is sufficient to consider an infinite beam since the localised shock response is attained before waves reach any reflecting termination.

Denote as $H(\omega,x)$ the FRF between any response quantity $q(t,x)$ at time t and position x arising from a transverse point force $f(t)$ acting at the origin. (A point moment excitation can be similarly treated). The time response to an arbitrary transient input is thus obtained,

$$q(t,x)=\mathrm{F}^{-1}\left(H(\omega,x)F(\omega)\right) \tag{15}$$

where $F(\omega)$ is the spectrum of $f(t)$ and $\mathcal{F}^{-1}$ denotes the Inverse Fourier Transform. Eq. (15) is solved in discrete time and frequency domains using the forward Fast Fourier Transform (FFT) and Inverse Fast Fourier Transform (IFFT).

The transient transverse velocity response of an infinite beam is obtained by adopting the transfer mobility for $H(\omega,x)$, i.e.

$$H(\omega,x)=\frac{V(\omega,x)}{F(\omega)}=\frac{-\omega}{4E^{*}Ik^{3}}\left(\mathrm{i}e^{-kx}-\mathrm{i}e^{-\mathrm{i}kx}\right) \tag{16}$$

where the exponential terms represent evanescent and propagating flexural waves. Damping, whilst omitted in the derivation of the excitation waveform in section 2, is now included by means of a complex Young's modulus

$$E^{*}=E\left(1+\mathrm{i}\eta(\omega)\right) \tag{17}$$

to account for wave attenuation, where $\eta(\omega)$ is the frequency dependent damping loss factor. A viscous damping model, for which $\eta(\omega)$ increases linearly with frequency, can be chosen to ensure that transient analyses are causal, although this may cause excessive attenuation at higher frequencies.

Displacement and acceleration responses can be similarly obtained from the transfer receptance and accelerance FRFs. Other response quantities of possible interest include stress and strain. The transfer FRF of normal surface strain to transverse force is derived in Appendix A as

$$\frac{\varepsilon(\omega,x)}{F(\omega)}=\frac{h}{8E^{*}Ik}\left(e^{-kx}-\mathrm{i}e^{-\mathrm{i}kx}\right) \tag{18}$$

Recalling the dispersion relation of Eq. (4), it is apparent that the velocity and strain based FRFs share the same frequency dependence, since strain energy and kinetic energy must remain in balance during free vibration.

Shear stress between an accreted layer and its substrate is the response quantity of interest for vibration based accretion removal [13]. Whilst zero at the surface of the single layer beam model adopted in this paper, the shear stress on the neutral axis is nevertheless a useful proxy measure in feasibility and optimisation studies. The transfer FRF of shear stress on the neutral axis to transverse force, for a rectangular beam, is derived in Appendix A as

$$\frac{\tau(\omega,x)}{F(\omega)}=-\frac{h^{2}}{32I}\left(e^{-kx}+e^{-\mathrm{i}kx}\right) \tag{19}$$

It is interesting to note that, aside from attenuation due to damping, the shear stress per unit force is independent of frequency in the far field. This characteristic can be expected to benefit the accumulated shock response over a frequency bandwidth.

In practice, mass loading might occur at the driving point owing to instrumentation such as a force gauge or accelerometer. This mass loading effect can be included in the model by appropriate modification of the FRF of interest. The transfer FRF of the mass-loaded beam, $H_{+}(\omega,x)$ is related to that of the bare beam $H(\omega,x)$ by

$$H_{+}(\omega,x)=\frac{H(\omega,x)}{1+m\alpha_{0}(\omega)} \tag{20}$$

where *m* is the added point mass and $\alpha_{0}(\omega)$ is the driving point accelerance of the bare beam, which is given by the derivative of Eq. (16) evaluated at $x=0$.

3.2 Actuator model

At frequencies significantly below the armature resonance, the mechanical elements of an electrodynamic shaker can be represented by a single degree-of-freedom system such that its accelerance is given by

$$\alpha_a(\omega) = \frac{-\omega^2}{-\omega^2 m_s + \mathrm{i}\omega c_s + k_s} \tag{21}$$

where, k_s, c_s, and m_s are the suspension stiffness, damping coefficient and moving mass of the shaker.

The electrical impedance of the shaker coil can be modelled as a resistor *R* in series with an inductor L_1, coupled to the mechanical shaker through back electromagnetic forces [14],

$$\frac{E(\omega)}{I(\omega)} = (R + \mathrm{i}\omega L_1) + \frac{1}{\mathrm{i}\omega} K_v K_f \alpha_a(\omega) \tag{22}$$

The scaling factors, K_v and K_f, in the electromechanical coupling term in Eq. (22) are the back EMF voltage constant and electromagnetic force constant. At high frequencies, the coupling term becomes mass controlled and the inductance dominates causing the magnitude of the impedance from the model to increase in proportion to frequency and the phase to tend to 90 degrees. However, in practice, the impedance is often observed to increase with $\sqrt{\mathrm{i}\omega}$ [15]. This phenomenon, caused by induced Eddy currents, can be modelled by semi-inductance. The analysis reported in [16] expresses this as an additional term to the impedance such that Eq. (22) becomes

$$\frac{E(\omega)}{I(\omega)} = (R + \mathrm{i}\omega L_1) + \frac{1}{\mathrm{i}\omega} K_v K_f \alpha_a(\omega) + \left(\frac{1}{\mathrm{i}\omega L_2} + \frac{1}{\sqrt{\omega} S} \right)^{-1} \tag{23}$$

where *S* is the semi-inductance and L_2 is an additional inductance parameter.

It should be noted that the additional impedance term in Eq. (23) could give rise to an acausal time response.

3.3 Coupling beam and actuator models

The spectrum of the input force $F(\omega)$ required in Eq. (15) can be related to the spectrum of the chirp input voltage $E(\omega)$ as follows,

$$F(\omega)=\frac{F(\omega)}{F_c(\omega)}.\frac{F_c(\omega)}{E(\omega)}.E(\omega) \tag{24}$$

where $F(\omega)/F_c(\omega)$ is the FRF between the force transmitted to the beam and force induced by the coil, and $F_c(\omega)/E(\omega)$ is the FRF between coil force and actuator voltage.

The FRF of force transmitted to the beam with respect to coil force is determined by the relative accelerances of the actuator and beam according to [14]

$$\frac{F(\omega)}{F_c(\omega)}=\frac{\alpha_a(\omega)}{\alpha_0(\omega)+\alpha_a(\omega)} \tag{25}$$

In cases where the beam is significantly less mobile that the shaker then $\left|F(\omega)/F_c(\omega)\right|\approx 1$, i.e. the shaker acts as a force source and does not mechanically filter the input spectrum.

The FRF of coil force with respect to actuator voltage is given by [14]

$$\frac{F_c(\omega)}{E(\omega)}=K_f\left(\frac{E(\omega)}{I(\omega)}\right)^{-1} \tag{26}$$

where $E(\omega)/I(\omega)$ is now the electrical impedance of the shaker when coupled to the structure, and is given by

$$\frac{E(\omega)}{I(\omega)}=(R+\mathrm{i}\omega L_1)+\frac{1}{\mathrm{i}\omega}K_v K_f\frac{\alpha_0(\omega)}{1+\dfrac{\alpha_0(\omega)}{\alpha_a(\omega)}}+\left(\frac{1}{\mathrm{i}\omega L_2}+\frac{1}{\sqrt{\omega}S}\right)^{-1} \tag{27}$$

4. Simulated results

Simulated results are presented from the analytical model of an infinite beam described in section 3, subjected to the chirp excitation of section 2. An ideal actuator is assumed in this section that faithfully reproduces the chirp waveform without any filtering, i.e. the actuator

behaves a force source and its electrical impedance is independent of frequency over the excitation bandwidth.

The material and geometric parameters were chosen for consistency with later experimental results in section 5. The beam was of rectangular cross section, 19.05 mm wide and 3.175 mm thick, and made from aluminium. Damping was initially omitted from the model. The dispersion relation in the form of group velocity against frequency is shown in Figure 1(a). The group velocity increases by a factor of ten over the two decades of 100 Hz to 10 kHz shown, in accordance with Eq. (7). Likewise, Figure 1(b) shows the dispersion relation as wavelength against frequency. The shortest wavelength is about 16 times the beam's thickness thereby ensuring the validity of Euler-Bernoulli beam theory. Frequency analysis was carried out with an FFT bandwidth of 65.536 kHz and an FFT size of 32768. The resulting 0.5 s record length was sufficient to avoid wrap-around effects in all cases.

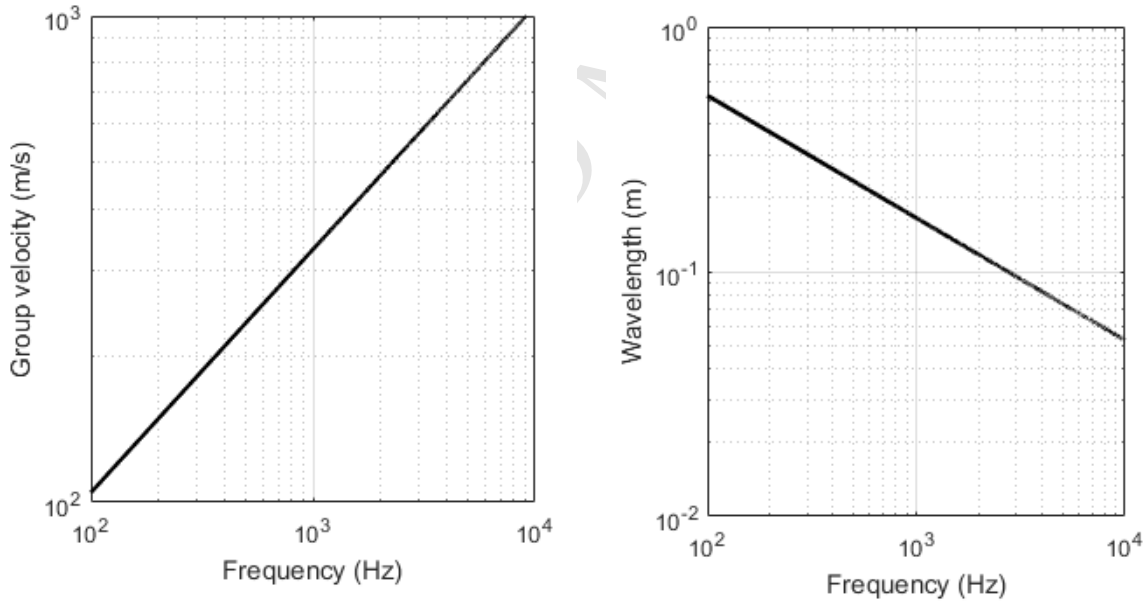

(a) (b)

Figure 1. Dispersion relation for beam (a) Group velocity and (b) Wavelength

4.1 Illustrative results

Figure 2(a) shows the required chirp waveform obtained from Eqns. (12) to (14) to synchronise the arrival of frequencies from 100Hz to 10kHz at the target focal point x_f at 2.5 m from the input at x=0. The chirp is preceded by a single cycle at the start frequency, the amplitude of which is increased linearly with time. The instantaneous frequency of the chirp, as given by Eq. (11), is shown in Figure 2(b). The duration of the chirp, 21 ms in this case, is determined by the group velocity of the start frequency and the distance to the focal point. The sweep rate is highly nonlinear resulting in a spectrum that rolls off at about 13dB per decade, as shown in Figure 3.

Figure 4(a) shows the velocity response at 2.51 m, where the peak velocity is largest, which is 0.01 m beyond the target focal point. The simultaneous arrival of the various frequency components manifests itself as an impulse of much shorter duration than the excitation waveform at the expected arrival time of 0.034 ms. This is preceded by an oscillation at the start frequency due to the initially ramped input. The acceleration response, shown in Figure 4(b), features a shorter pulse in which high frequencies are more apparent since accelerance scales with $\omega^{\frac{1}{2}}$. The maximum peak acceleration occurs 2.46 m from the force position owing to the 90° phase shift in the FRF.

Figure 5 shows the positive and negative peaks of the velocity and acceleration responses as functions of distance along the beam. Whilst the largest peak is at or near the nominal focal point there are other local maxima, particularly in the acceleration response which is dominated by higher frequencies. Large positive accelerations generally coincide with small negative accelerations, and vice versa. Movie animations of the disturbances travelling along the beam are available to view [17], the peak-hold averages of which form the plots shown in Figure 5.

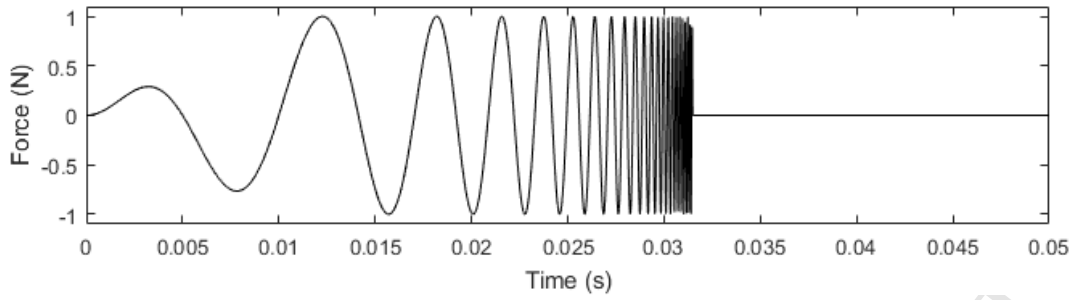

(a)

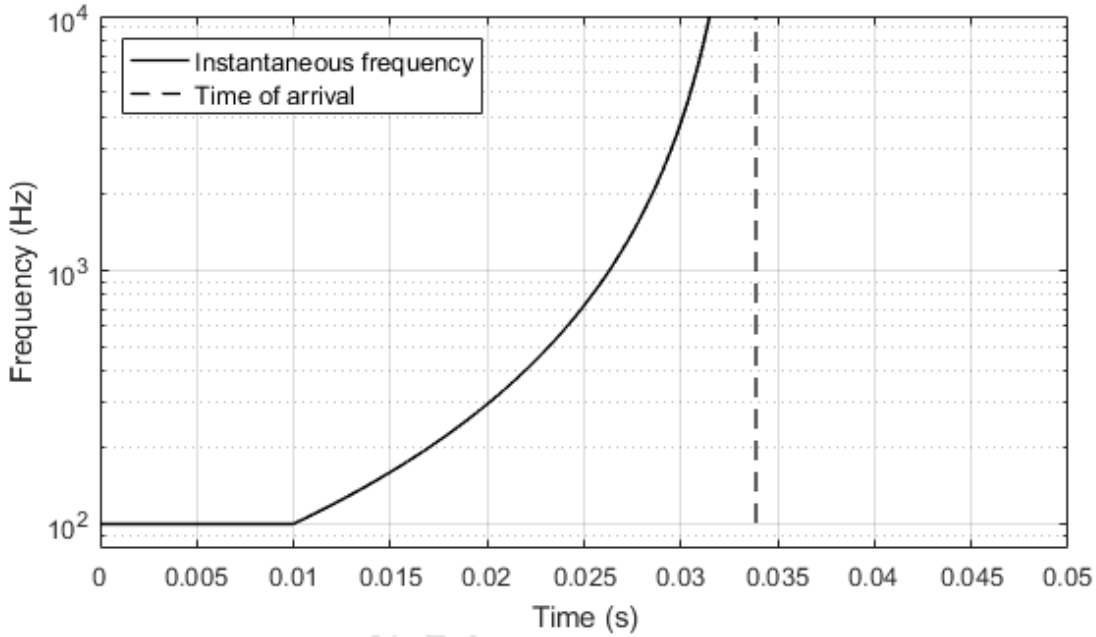

(b)

Figure 2. Chirp excitation signal. (a) waveform, and (b) instantaneous frequency as a function of time

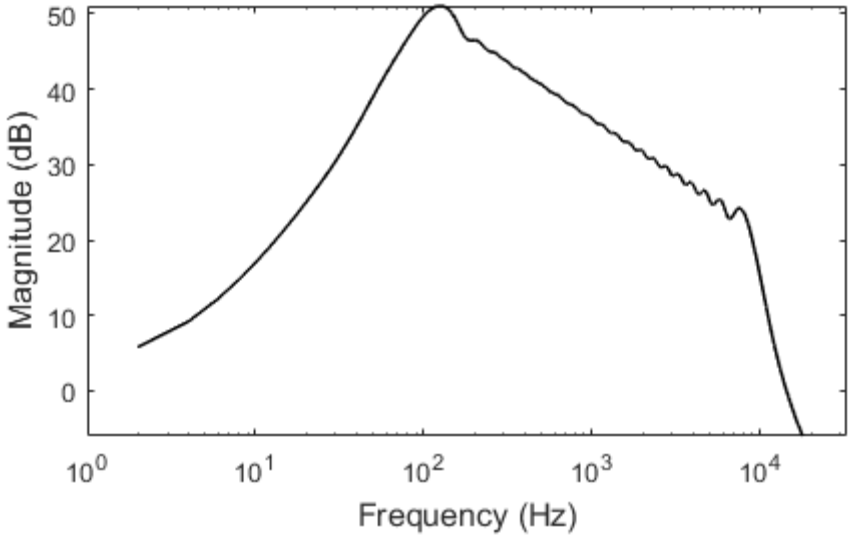

Figure 3. Spectrum of chirp excitation

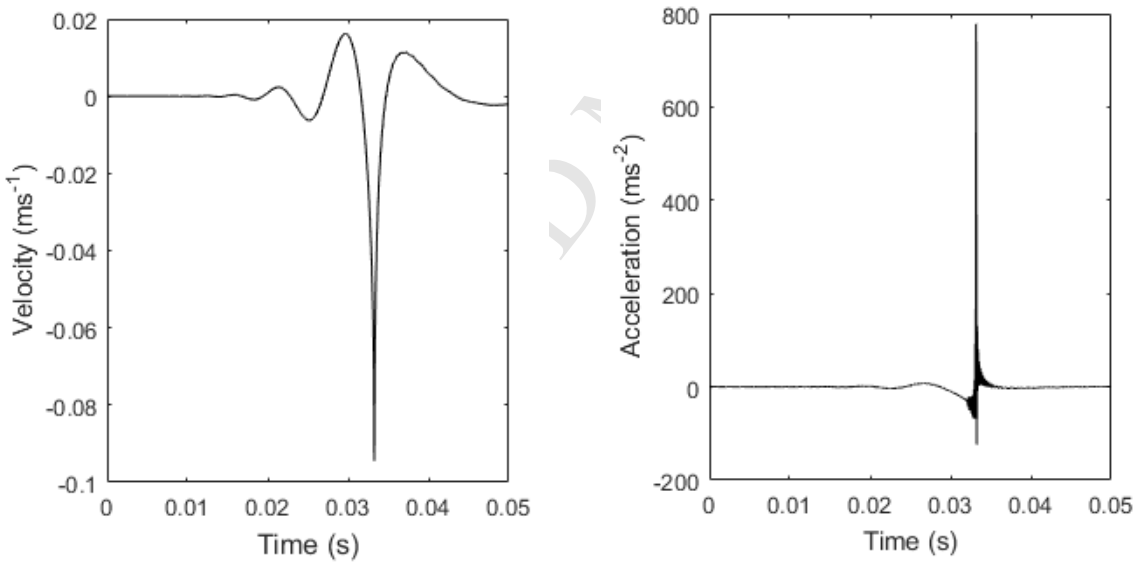

(a) (b)

Figure 4. Time response at position where peak response is a maximum. (a) Velocity at 2.51 m, and (b) acceleration at 2.46 m

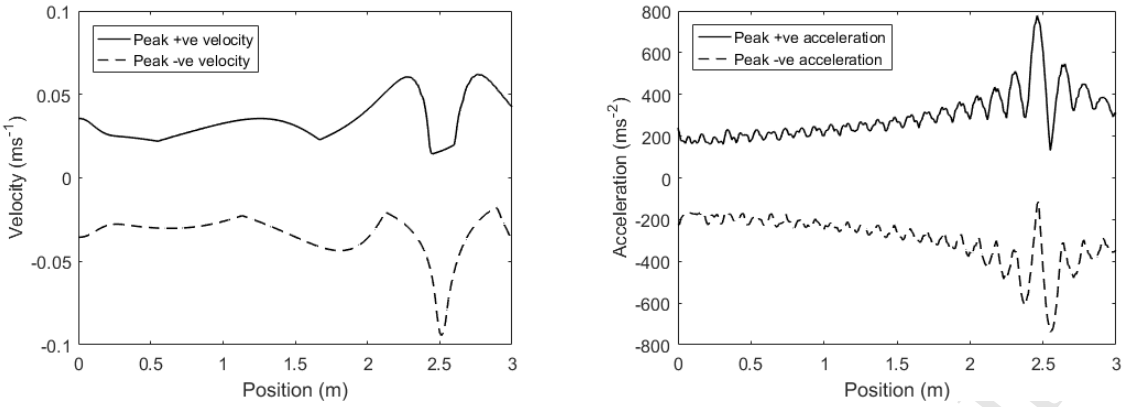

(a) (b)

Figure 5. Peak responses as a function of position along the beam. (a) Velocity and (b) acceleration

A convenient measure of the amplification afforded by the chirp excitation is the ratio of the highest peak response to the maximum steady state harmonic response at the same position over the bandwidth of the chirp, i.e.

amplification factor, $$AF = \frac{q\left(t_m, x_m\right)}{\max_{\omega\in[\omega_0,\omega_T]}\left(\dfrac{Q\left(\omega, x_m\right)}{F\left(\omega\right)}\right)} \tag{28}$$

where, $$\left(t_m, x_m\right) = \arg\max\left(\max\left(q\left(t,x\right)\right), -\min\left(q\left(t,x\right)\right)\right) \tag{29}$$

The amplification factors for the velocity and acceleration results shown in Figure 5(a) and (b) are 3.32 and 4.35 respectively.

4.2 Variation of chirp bandwidth

The effect of bandwidth was investigated by varying the chirp's lower and upper frequencies independently. First the lower frequency of the chirp was fixed at 100 Hz and the upper frequency was increased from 200 Hz to 10 kHz. The nominal focal point was set to 2.5 m as before, and damping was omitted. The resulting amplification factors for velocity, acceleration, shear strain and normal strain as defined in Eq. (28) are shown in Figure 6(a). For all response quantities the amplification factor increases as the upper frequency of the chirp is increased, since more energy is input. Shear stress at the neutral axis is amplified most, rising to a factor of 10, on account of its flat frequency response given in Eq. (19).

Figure 6(b) shows the amplification factor when the upper frequency of the chirp is fixed at 10 kHz and the lower frequency is increased in octaves from 100 Hz to 6.4 kHz. With the exception of shear stress, there is little to be gained from chirping below 1 kHz, and an amplification factor of about 4 can be achieved from a bandwidth of 1 kHz to 10 kHz. In practice, actuator bandwidth is also a limiting factor, as explored in section 5.

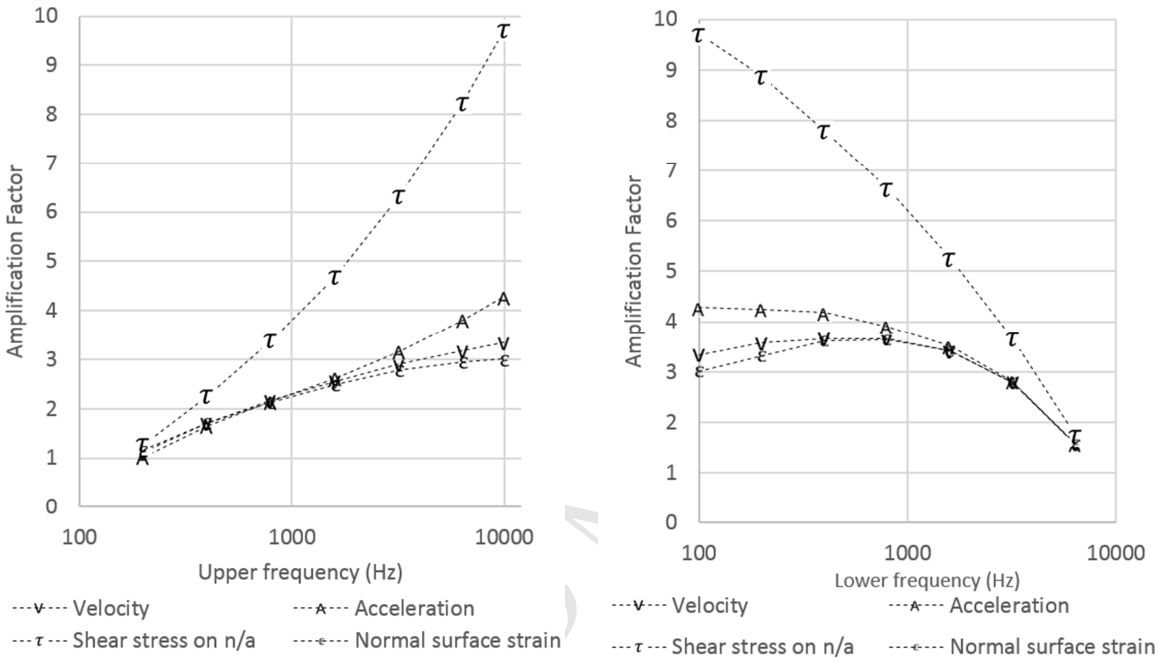

(a) (b)

Figure 6. Amplification factor as a function of (a) chirp end frequency for a fixed start frequency of 100Hz, and (b) chirp start frequency for a fixed end frequency of 10kHz

4.3 Variation of focal distance

A fixed bandwidth of 1 kHz to 10 kHz was selected to investigate the effect of increasing the nominal focal distance from the driving point to a distance of 100 m. Damping is again omitted. Figure 7 shows the amplification factor for all four response quantities. In each case amplification increases with distance and all curves closely follow a power law with an exponent close to 0.5. The reason for the improvement arises from the difference in flight times between the slowest and fastest frequency components, which increases with distance, allowing a greater duration of the chirp excitation and corresponding energy input.

The shear stress is again amplified most owing to its flat frequency response. The velocity and normal strain results overlay since their FRFs with respect to transverse force both vary with $\omega^{-\frac{1}{2}}$.

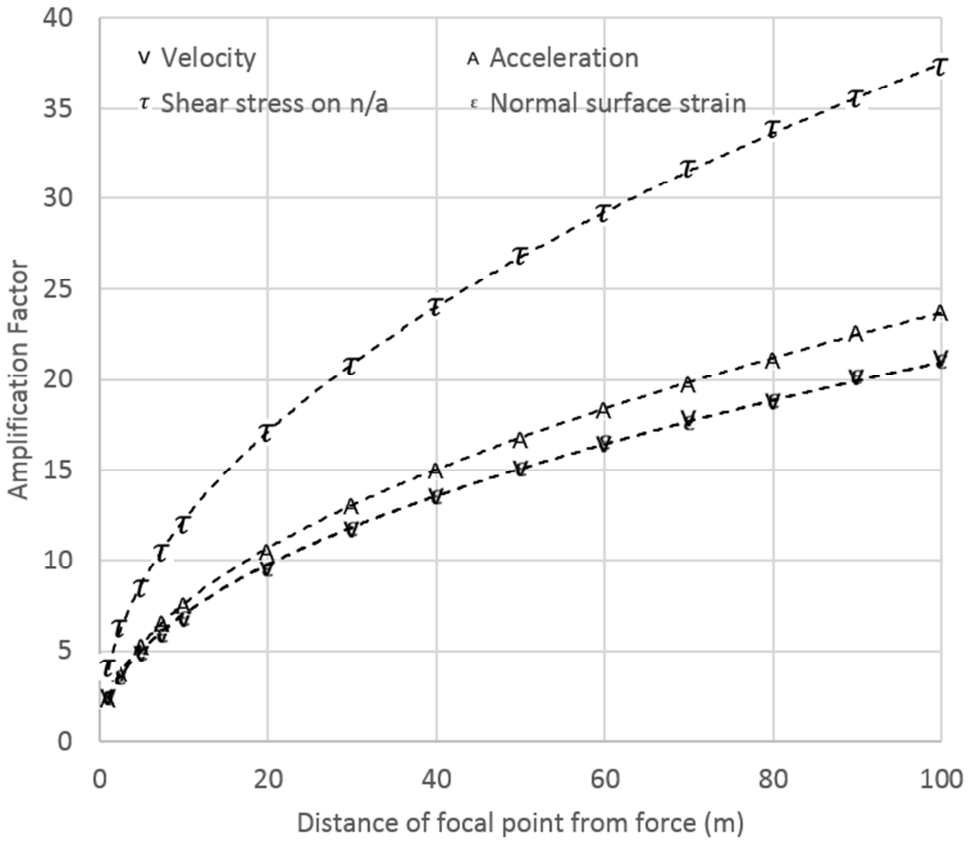

Figure 7. Amplification factor as a function of position of focal point along undamped beam. The dashed lines indicate power law fits to the data

4.4 The effect of structural damping

Figure 8 illustrates the effect of applying damping to the beam. The damping loss factor was set to vary linearly between 0.1% at 1 kHz and 1% at 10 kHz, the start and end frequencies of the chirp, in order to ensure a causal response. Attenuation is responsible for curtailing amplification significantly, particularly beyond 5 m from the force. When the damping loss

factor was increased ten-fold (results omitted for brevity) focussing was not possible beyond 5m.

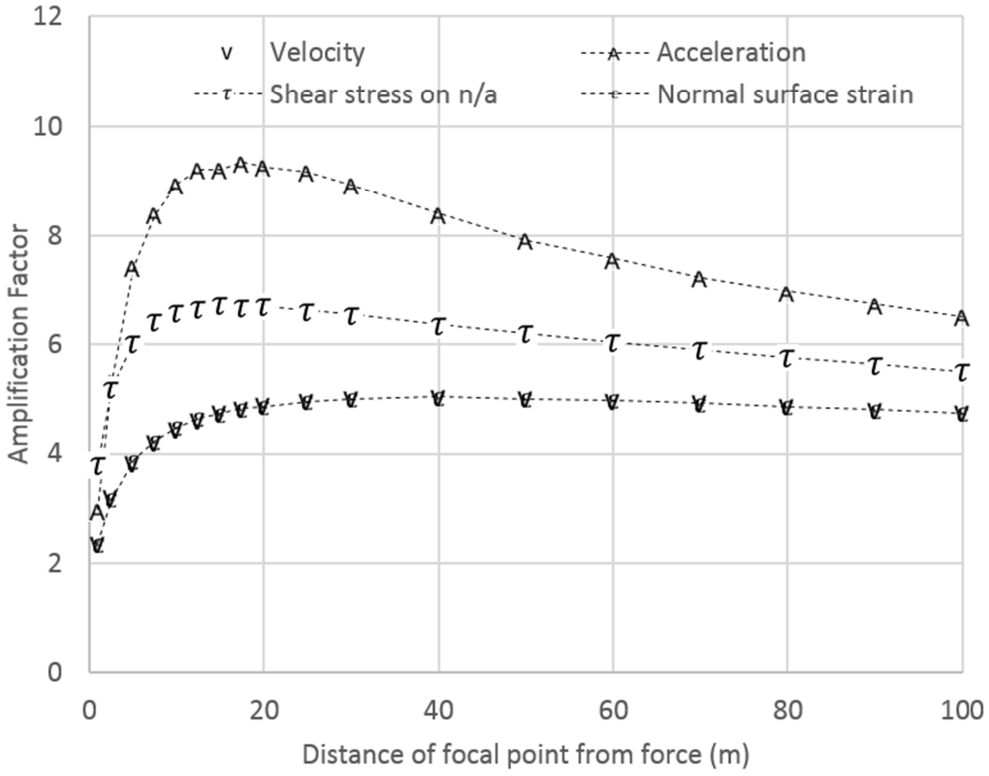

Figure 8. Amplification factor as a function of position of focal point along damped beam

5. Experimental validation

Practical implementation of the chirp excitation requires selection and deployment of an electromechanical actuator. The dynamic response depends on the frequency response of the structure coupled to the actuator which, for generality, was not considered in section 4. For the purpose of experimental implementation, an electrodynamic shaker was selected, and validation of the coupled model described in section 3 was sought.

The rig comprised a 5 m long aluminium beam suspended at several points along its length. Its ends were buried in boxes of dry 'silver sand' to approximate anechoic terminations, giving a working section of about 3.5 m. The physical arrangement is depicted schematically in Figure 9. The beam has a solid rectangular cross section of width 19.05 mm and thickness

3.175 mm, which is consistent with previous simulations. The beam was excited using an electrodynamic shaker (Data Physics V4) powered by a power amplifier (Data Physics PA30E). The shaker was attached to the centreline of the beam, at about 0.5 m from the entrance to one of the sand boxes, via a short stinger. A force gauge (PCB 208C01) was mounted directly on the beam to measure the transmitted force, and the terminal voltage and current draw of the shaker coil could be measured. The responses at remote positions on the beam were measured using a roving miniature accelerometer (PCB 352C22).

This section first presents frequency domain experimental validations of the beam and the shaker models described in sections 3.1 and 3.2. The transient responses of the coupled electromechanical system, reported in section 3.3, are then compared under chirp excitations of the form proposed in section 2.

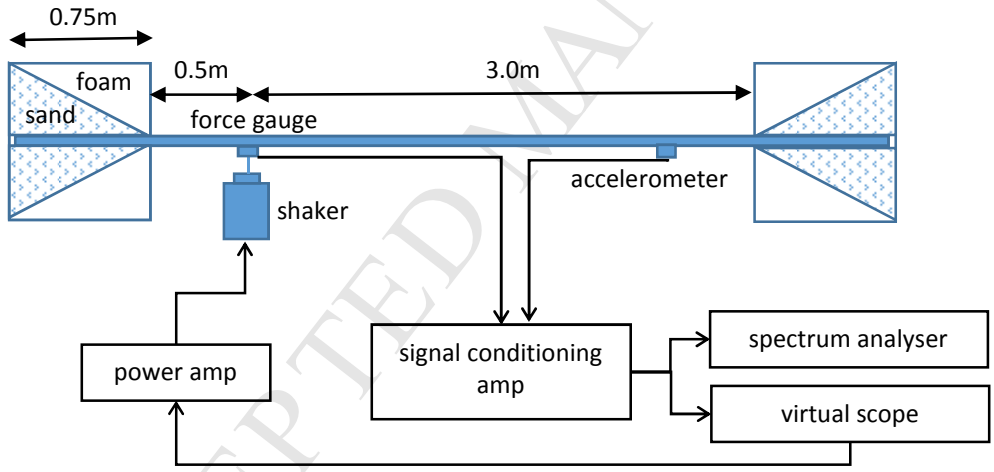

Figure 9. Schematic of experimental rig

5.1 Validation of beam model

The beam model presented in section 3 was validated initially in terms of its free wave propagation, followed by its forced response.

The dispersion curve for flexural waves was measured in the standard way [18] using three transfer accelerances $H_1(\omega)$ to $H_3(\omega)$ that were equally spaced in the far field of the shaker and sand boxes. An estimate of the wavenumber *k* is given by

$$\cos k\Delta = \tfrac{1}{2}\left(\frac{H_1(\omega)}{H_2(\omega)} + \frac{H_3(\omega)}{H_2(\omega)}\right) \tag{30}$$

A sensor spacing of 0.03 m was selected, less than half of the shortest wavelength in the bandwidth of interest. Figure 10 shows the measured dispersion curve overlaid with that expected from Euler-Bernoulli theory and defined in Eq. (4). The nominal material properties for aluminium (Young's modulus of 68 GPa and density of 2700 kgm^{-3}) and beam cross-section geometry used in the model give good agreement and no tuning of the parameter values was deemed necessary.

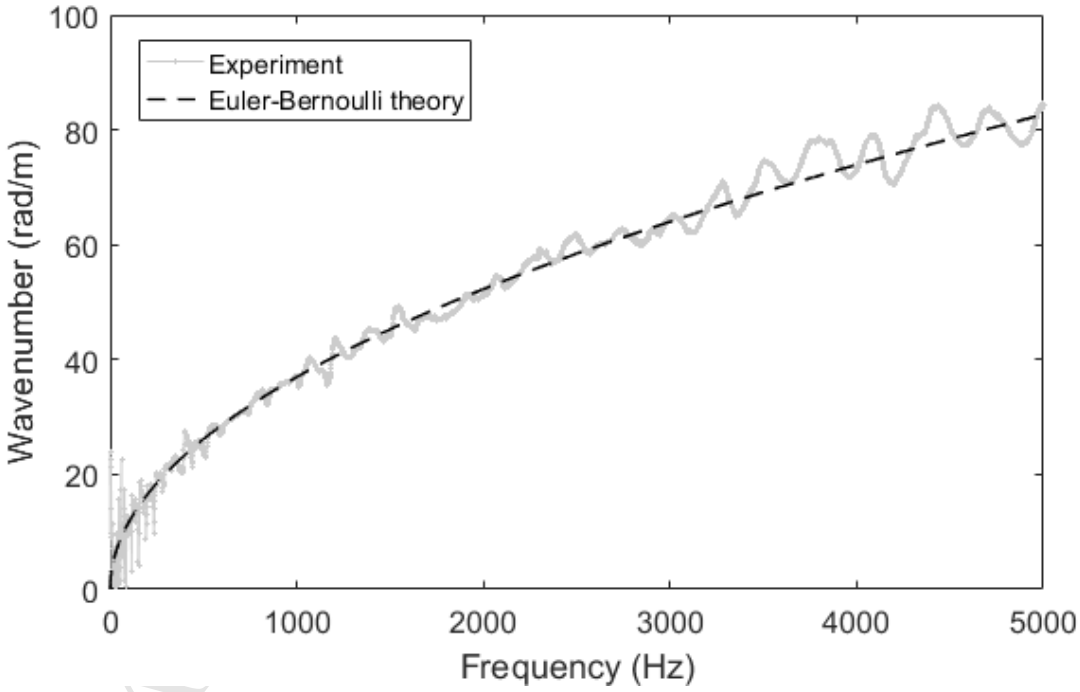

Figure 10. Dispersion relation for aluminium beam

The accelerometer was positioned at the origin to measure the driving point accelerance, the magnitude of which is shown in Figure 11. Strong resonant behaviour is apparent at lower frequencies, particularly below 400 Hz, since flexural waves of long wavelength are poorly attenuated by the sandboxes. Above 1000 Hz, the beam behaves almost as if infinite

in length, although the accelerance does not increase with 10 dB per decade, as expected of a bare beam, due to mass loading by the force gauge.

The value of the attachment mass was adjusted in the model to achieve a satisfactory agreement with the measured driving point accelerance, which is shown in Figure 11. The selected value of 11.25 g is consistent with the mass of the light side of the force gauge together with its attachment stud.

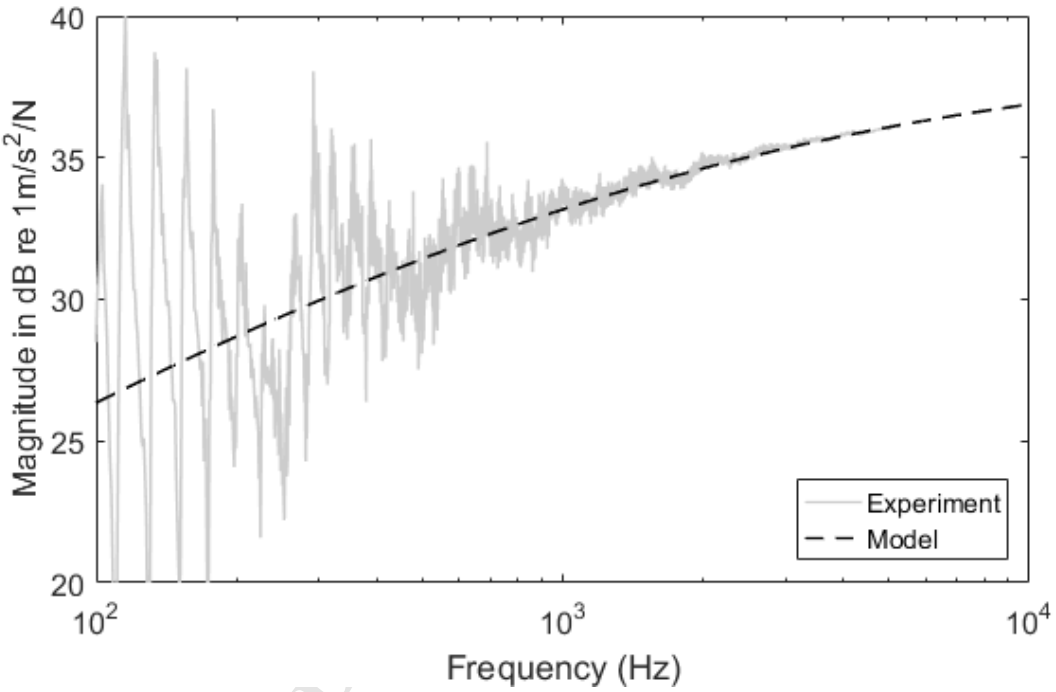

Figure 11. Comparison of driving point accelerance between infinite beam model with 11.25 g attachment mass and experimental beam terminated in sand boxes

5.2 Validation of shaker model

Vibration tests were carried out on the shaker when disconnected from the structure to characterise its dynamic behaviour. The base of the shaker was grounded both for these tests and when used to excite the structure. Figure 12(a) shows the measured accelerance of the shaker's armature, as measured with an impact hammer, when the coil was open-circuit. The single degree-of-freedom model outlined in section 3.2 was fitted to the data to determine the shaker's suspension stiffness, damping coefficient and moving mass. Figure

12(b) shows the FRF of acceleration to coil current from which the electromagnetic force constant was estimated. The parameter estimates are listed in Table 1 and the frequency responses of the fitted model are overlaid in the figures.

The electrical impedance of the unconnected shaker was also measured. Eq. (23) was fitted to the measured data manually to obtain estimates for the resistance, inductance and coupling constants, and their values are listed in Table 1.

Figure 13(a) and (b) show the measured impedance of the coil overlaid with the result predicted by Eq. (23) using the estimated parameter values. The semi-inductance model accurately captures the frequency dependence of both the magnitude and phase of the impedance.

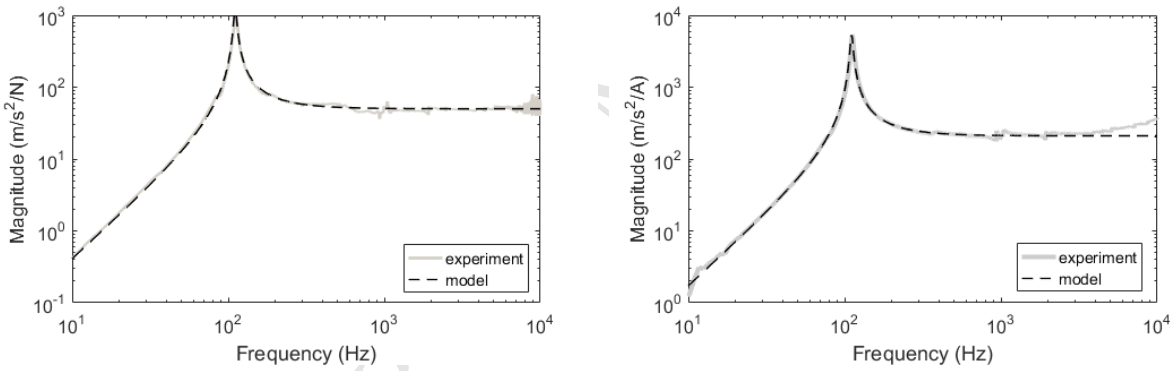

(a) (b)

Figure 12. Frequency response functions of shaker. (a) acceleration to force, and (b) acceleration to current.

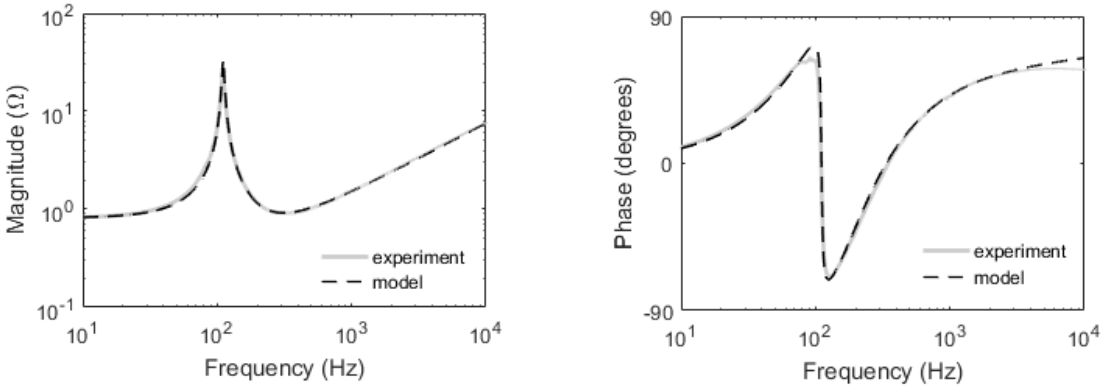

(a) (b)

Figure 13. Electrical impedance of the shaker. (a) Magnitude and (b) Phase.

.

Parameter	Value
Suspension stiffness, k_s	9.7 kNm^{-1}
Damping coefficient, c_s	0.55 Nsm^{-1}
Moving mass, m_s	0.020 kg
Resistance, *R*	0.82 Ω
Inductance, L_1	5.0× 10^{-5} H
Inductance, L_2	2.5× 10^{-4} H
Semi-inductance, *S*	23× 10^{-3} semihenries
Electromagnetic force constant, K_f	4.2 NA^{-1}
Back EMF voltage constant, K_V	4.2 Vsm^{-1}

Table 1. Parameter value estimates for the electrodynamic shaker (Data Physics V4)

5.3 Validation of transient response

A chirp excitation was implemented, using Eq. (12) to (14), intent on producing a peak response at a nominal distance of 2.50 m from the shaker. A linear ramp of three cycles was included to reduce unwanted transients at the start of the chirp. The bandwidth selected for the chirp was from 500 Hz, below which the beam is strongly resonant, to 5 kHz above which the shaker model begins to deviate from the measured behaviour. A virtual scope

(Picoscope 3203D) was used to acquire the shaker terminal voltage and the accelerometer signal for each of ten or more chirp events and compute the mean of the maxima and minima for both channels. The force gauge was retained primarily to avoid altering the dynamics of the system from its previously validated state, and its signal acquired only for occasional diagnostic purposes. The presence of the force gauge and stinger mass-loaded the shaker's armature by 32 g in addition to the 11.25 g loading to the beam that was quantified in section 5.1, both of which were accounted for in the model in accordance with Eq. (20).

The accelerometer was moved along a 2.7 m length of the beam in increments of 20 mm. At each position the maximum and minimum accelerations were noted together with the maximum input voltage. Figure 14 shows the maximum and minimum accelerations per peak voltage as a function of distance along the beam. The measured results are overlaid with predictions from the electromechanical model using the validated parameter values reported in Table 1. The results are in very close agreement.

The maximum positive and negative peaks occur at 2.42 m and 2.56 m respectively, either side of the nominal focal point. The peak values are about three times larger than those just outside the nearfield, at about 0.2 m from the shaker, which is a qualitative measure of the amplification achieved through focussing of propagating waves. The model predicts a value for the amplification factor, as defined by Eq. (28), of 2.96. This value increases to 4.90 (results not presented for brevity) when the actuator model is replaced by a force source that perfectly replicates the excitation waveform, as assumed in section 4.

A key requirement for effective amplification is relative flatness of the system's frequency response over the bandwidth of the chirp such that a broad range of frequencies contribute non-negligibly to the response. Figure 15 shows the magnitude of the FRF of the driving point acceleration to input voltage. The resonant region below 500Hz could be exploited but was excluded for validation purposes since the beam is modelled as infinite. Over a 500 Hz to 5 kHz bandwidth the gain drops by 11 dB in the model, and 7 dB in the experiment, which curbs contributions from higher frequencies. Contrary to the model, the subsequent gain increase in the experimental result suggests that additional benefit can be obtained by increasing the upper frequency to 10 kHz.

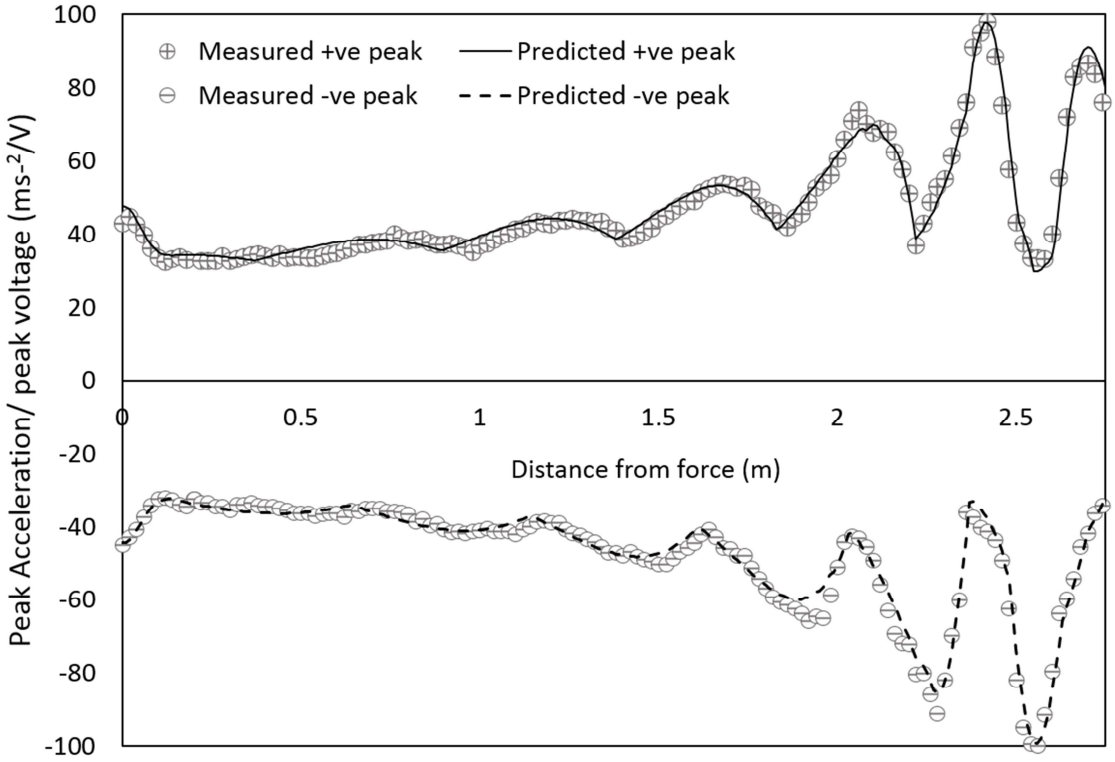

Figure 14. Peak acceleration per volt as a function of distance along beam from shaker

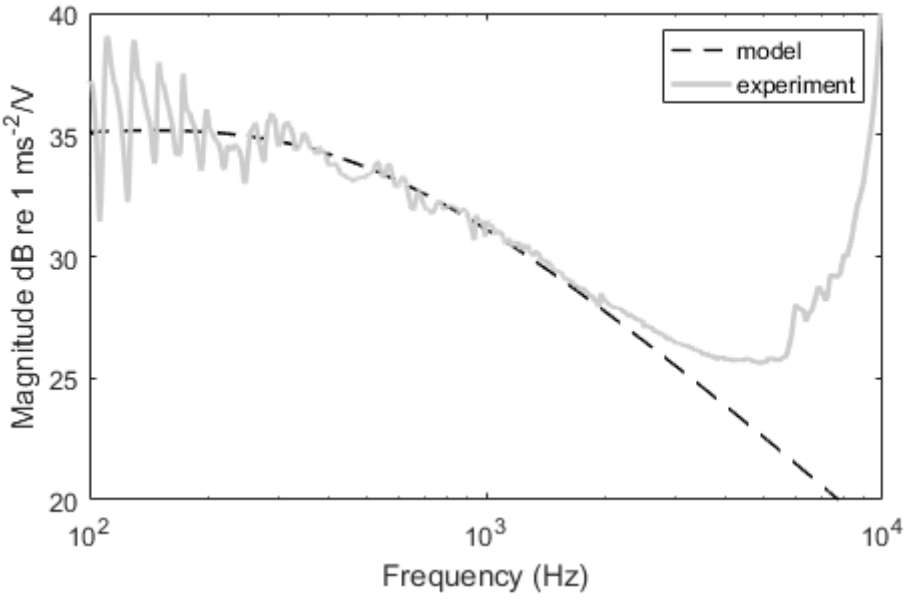

Figure 15. FRF between acceleration at driving point and shaker voltage.

6. Conclusions

An analytical expression has been presented for a chirp waveform that excites flexural waves so as to produce a shock response at or close to an arbitrarily chosen position on a beam or plate. The technique works by compensating for wave dispersion through prior knowledge of the dispersion relation. Chirp excitations have been applied to an analytical frequency domain model for a beam and the results transformed to the time domain. In the absence of damping the peak response is found to increase approximately with the square root of distance from the input force. In practice, this effect is negated at larger distances by attenuation due to damping.

The chirp technique has been implemented experimentally on a beam driven by an electrodynamic shaker. Measured results are in close agreement with the model when shaker dynamics are included. A shock response is realised close to the intended location which is about three times larger than the peak amplitude due to harmonic excitation. Higher performance is possible depending on the response quantity of interest and the flatness of its frequency response with respect to the electrical or mechanical input. The amplified response does not rely on any resonance of the actuator or structure, is localised and tuneable in real time.

A potential application of the technique, which is the subject of ongoing studies, is the removal of accretions from structures using high amplitude dispersive waves. Although the current analytical formulation is limited to flexural waves in uniform beam or plate sections where an equivalent bending stiffness can be assumed, computation of the chirp waveform by either the same approach, or that described in [1], is in principle possible for other wave types for which the dispersion relation is known numerically.

Acknowledgements

The author acknowledges the financial support of the Engineering and Physical Sciences Research Council under grant EP/M005321/1. Roger Pinnington's contribution, as supervisor of the dissertation [8] from which this work developed, is gratefully

acknowledged. Sincere thanks are due to Hiten Mulchandani for checking many aspects of the model during its subsequent development in follow-on research activities.

Appendix A

The transfer receptance FRF of an infinite Euler-Bernoulli beam excited at $x = 0$ is given by [11]

$$\frac{W(\omega, x)}{F(\omega)} = \frac{-1}{4E^* Ik^3}\left(e^{-kx} + \mathrm{i}e^{-\mathrm{i}kx}\right) \tag{A.1}$$

The bending moment at position *x* is

$$M(x) = -E^* I \frac{d^2 W}{dx^2} \tag{A.2}$$

Substituting for *W* from Eq. (A.1) into Eq. (A.2), the FRF of dynamic bending moment to transverse force is obtained as

$$\frac{M(\omega, x)}{F(\omega)} = \frac{1}{4k}\left(e^{-kx} - \mathrm{i}e^{-\mathrm{i}kx}\right) \tag{A.3}$$

Dynamic normal strain at a distance *y* from the neutral axis is given by

$$\varepsilon(\omega, x) = \frac{M(\omega, x)\, y}{EI} \tag{A.4}$$

where $y = \frac{1}{2}h$ for strain on the surface of a symmetric cross section. Substituting for *M* from Eq. (A.3) into Eq. (A.4) gives the FRF of surface normal strain to transverse force as

$$\frac{\varepsilon(\omega, x)}{F(\omega)} = \frac{h}{8E^* Ik}\left(e^{-kx} - \mathrm{i}e^{-\mathrm{i}kx}\right) \tag{A.5}$$

Differentiating Eq. (A.3) with respect to *x* yields the FRF for the vertical shear force *S* as

$$\frac{S(\omega,x)}{F(\omega)} = -\frac{1}{4}\left(e^{-kx} - e^{-\mathrm{i}kx}\right) \tag{A.6}$$

The horizontal shear stress is related to the vertical shear force by

$$\tau = \frac{SI_1(y)}{Ib} \tag{A.7}$$

where, for a rectangular cross section of width *b,*

$$I_1(y) = \frac{b}{2}\left(\frac{h^2}{4} - y^2\right) \tag{A.8}$$

represents the first moment of the cross section area that lies a distance larger than *y* from the neutral axis, which attains a maximum value on the neutral axis of $I_1(0) = bh^2/8$.

Substituting for $S(\omega,x)/F(\omega)$ and $I_1(0)$ into Eq. (A.8) gives

$$\frac{\tau(\omega,x)}{F(\omega)} = -\frac{h^2}{32I}\left(e^{-kx} + e^{-\mathrm{i}kx}\right) \tag{A.9}$$

References

[1] L. Zeng, J. Lin, Chirp-based dispersion pre-compensation for high resolution Lamb wave inspection, NDT&E International 61 (2014) 35-44.

[2] J. Palacios, A review of ultrasonic vibration for de-icing of aircraft, International Conference on Vibration and Vibro-acoustics, China, January 2014.

[3] M. Fink, Time reversed acoustics, Physics Today, 50, (1997), 34-40.

[4] M. Fink, Time reversal of ultrasonic fields. 1. Basic principles, IEEE transaction on ultrasonics ferroelectrics and frequency control, Volume: 39 Issue: 5 (1992), 555-566.

[5] G. Montaldo, P. Roux, A. Derode, C. Negreira, M. Fink, Generation of very high pressure pulses with 1-bit time reversal in a solid waveguide, J. Acoust. Soc. Am. 110, (2001), 2849-2857.

[6] S. Dion., L.P. Riel., M. Brouillette, Shock wave generation through constructive wave amplification. In: Kontis K. (eds) 28th International Symposium on Shock Waves. Springer, Berlin, Heidelberg (2012).

[7] D. Francoeur, A. Berry, Time reversal of flexural waves in a beam at audible frequency, J. Acoust. Soc. Am. 124 (2), (2008), 1006-1017.

[8] O. Kwon, Measurement of the wavenumber dispersion relationship in a resonant dispersive structure by signal shaping, MSc dissertation, ISVR, University of Southampton (1995).

[9] A. Brandt, Noise and vibration analysis: signal analysis and experimental procedures, Wiley 2011.

[10] J.E. Michaels, Sang Jun Lee, A.J. Croxford, P.D. Wilcox, Chirp excitation of ultrasonic guided waves, Ultrasonics 53 (2013), 265-270.

[11] K.F. Graff, Wave motion in elastic solids, Dover Publications, 1975.

[12] L. Cremer, M. Heckl, E.E. Ungar, Structure-borne sound, Springer-Verlag, 1973.

[13] M. Kalkowski, T.P. Waters, E. Rustighi, Delamination of surface accretions with structural waves: piezo-actuation and power requirements, Journal of Intelligent Materials Systems and Structures (2016), 1-20.

[14] K.G. McConnell, P.S. Varoto, Vibration testing theory and practice 2nd edition, Wiley, 2008. (Chapter 6)

[15] J. Vanderkooy, A model of loudspeaker driver impedance incorporating Eddy currents in the pole structure, J. Audio Eng. Soc., 37(3), (1989), 119-128.

[16] B. Lütkenhöner, What the electrical impedance can tell about the intrinsic properties of an electrodynamic shaker, PL0S ONE 12(3): e0174184, (2017).

[17] [dataset] T.P. Waters, Animations of a chirp waveform propagating along a beam, 2018, http://dx.doi.org/10.5258/SOTON/xxxxx (TBC).

[18] B. Zhang, T.P. Waters, B.R. Mace, Identifying joints from measured reflection coefficients in beam-like structures with application to a pipe support, Mechanical Systems and Signal Processing, 24(3), (2010), 784-795.